ACS APPLIED MATERIALS & INTERFACES

Research Article

www.acsami.org

Orientation and Alignment Control of Microphase-Separated PS-*b*-PDMS Substrate Patterns via Polymer Brush Chemistry

Dipu Borah,[†,‡,§] Sozaraj Rasappa,[†,‡] Ramsankar Senthamaraikannan,[†,‡] Barbara Kosmala,[†,§] Matthew T Shaw,[†,‡,§,∇] Justin D Holmes,[†,‡,§] and Michael A Morris*[,†,‡,§]

[†]Materials Chemistry Section, Department of Chemistry, University College Cork, College Road, Cork, Ireland

[‡]Centre for Adaptive Nanostructures and Nanodevices (CRANN), Trinity College Dublin, College Green, Dublin 2, Ireland

[§]Tyndall National Institute, Lee Maltings, Prospect Row, Cork, Ireland

[∇]Intel Ireland Limited, Collinstown Industrial Estate, Leixlip, Co. Kildare, Ireland

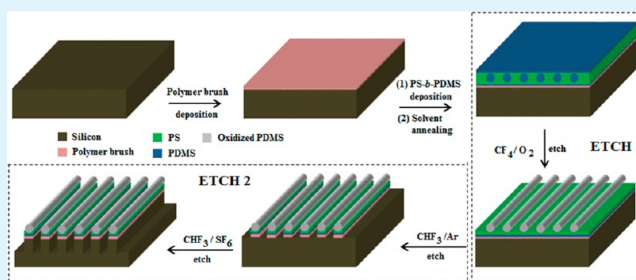

ABSTRACT: Block copolymer (BCP) microphase separation at substrate surfaces might enable the generation of substrate features in a scalable, bottom-up fashion, provided that the pattern structure, orientation, and alignment can be strictly controlled. The PS-*b*-PDMS (polystyrene-*b*-polydimethylsiloxane) system is attractive because it can form small features and the two blocks can be readily differentiated during pattern transfer. However, PS-*b*-PDMS offers a considerable challenge, because of the chemical differences in the blocks, which leads to poor surface wetting, poor pattern orientation control, and structural instabilities. These challenges are considerably greater when line patterns must be created, and this is the focus of the current work. Here, we report controlled pattern formation in cylinder-forming PS-*b*-PDMS by anchoring different types of hydroxyl-terminated homopolymer and random copolymer brushes on planar and topographically patterned silicon substrates for the fabrication of nanoscale templates. It is demonstrated that non-PDMS−OH-containing brushes may be used, which offers an advantage for substrate feature formation. To demonstrate the three-dimensional (3-D) film structure and show the potential of this system toward applications such as structure generation, the PDMS patterns were transferred to the underlying substrate to fabricate nanoscale features with a feature size of ~14 nm.

KEYWORDS: *polymer brushes, PS-b-PDMS, solvent anneal, self-assembly, graphoepitaxy, etching, nanoscale templates*

■ INTRODUCTION

The development of microtechnology and nanotechnology depends on the ability to fabricate microsized and nanosized structures with high precision. Top-down lithographic techniques include UV,[1] thermal,[2] e-beam,[3,4] and X-ray[5] methods, and the manufacturing, state-of-the-art, feature size is now ~16 nm. In parallel to the physical engineering of substrate features, the bottom-up approach, based on hierarchical self-assembly of structures ranging from molecular building blocks to nanoparticulates and macromolecular structures, is the subject of intense research.[6] There are advantages and drawbacks in both approaches. In top-down methodologies, further downsizing is critically related to light wavelengths, light-material interactions, and thermal management.[1,7,8] On the other hand, it is highly challenging to achieve long-range translational order and sufficient pattern robustness of systems fabricated with bottom-up approaches.[9−11]

Directed self-assembly (DSA) based on graphoepitaxy is a technique that exploits the complementarity of the two approaches.[12−15] The confinement of BCP structures within narrow, topographical features can guide BCP patterns into alignment and was first reported by Li et al. for polystyrene-*block*-polymethyl methacrylate (PS-*b*-PMMA).[16] Many authors have subsequently studied this system, because it is compatible with established resist technologies.[17,18] However, PS-*b*-PMMA has a relatively low Flory−Huggins parameter (χ) and results in minimum feature size dimensions that are well above that of the UV-lithography method. Other polymers can exhibit lower minimum feature size and polystyrene-*block*-polydimethylsiloxane (PS-*b*-PDMS) is attracting much research effort. This is because its Flory−Huggins parameter ($\chi = 68/T - 0.037$) is relatively high, allowing sub-10 nm feature size scaling,[19] as demonstrated for line-forming nonsymmetric PS-*b*-PDMS, using a nanoimprint lithography (NIL)-assisted DSA approach.[20] A further attractive feature of this system is its chemistry and composition, which allows it to be processed relatively easily into an on-chip etch mask that can be used for pattern transfer by selective etch methods.[21,22]

However, in the PS-*b*-PDMS system, two major issues arise: strong surface dewetting due to its high hydrophobicity and

Received: September 28, 2012
Accepted: December 10, 2012
Published: December 10, 2012

© 2012 American Chemical Society

difficulties in controlling feature orientation, particularly for definition of parallel versus vertical cylinder alignment. To overcome these limitations, a surface pretreatment with a PDMS−OH brush is usually required.[21,22] However, it should be noted that the use of a PDMS−OH brush may present further problems for pattern transfer into the substrate. Briefly, the PDMS−OH brush layer produces (on its own or with the BCP) a PDMS layer at the substrate−polymer interface, and this will increase the thickness of the surface passive silica layer and minimize the effectiveness of any selective Si:SiO_2 dioxide etch chemistry used for pattern transfer.[23] However, to tune the surface chemistry of the substrate to improve wetting characteristics of the BCP, and to confer orientational control of the pattern, reports of the use of other hydroxyl-terminated homopolymer and copolymer brushes as an alternative to the PDMS−OH brush is scant.[22] In order to address the deficit in alternative non-PDMS−OH-containing brush chemistry, hydroxyl-terminated homopolymer and copolymer brushes with different characteristics were investigated at both planar and topographically patterned substrates.

■ EXPERIMENTAL SECTION

Materials. The planar substrates used were polished, test grade reclaimed 8-in. silicon ⟨100⟩ wafers (*p*-type, B-doped, 650 μm thick, and resistivity of 6−14 Ω cm) with a native oxide layer of ∼2 nm. No attempt was taken to remove the native oxide. The topographically patterned substrates (fabricated via 193-nm UV lithography) were etched Si⟨100⟩ wafers with an insulating SiO_2 layer of 150 nm. The channel width and depth were 280 and 60 nm, respectively. Hydroxyl-terminated polystyrene (PS), polymethyl methacrylate (PMMA), polydimethylsiloxane (PDMS), a random copolymer composed of styrene (S), and methyl methacrylate (MMA) (PS-*r*-PMMA) and an asymmetric, cylinder-forming PS-*b*-PDMS diblock copolymer were all purchased from Polymer Source, Inc., Canada, and used as-received. Detailed descriptions of the polymers are summarized in Table 1. Toluene (99.8%, anhydrous), sulfuric acid (98%), and hydrogen peroxide (30%) were purchased from Sigma−Aldrich and used without further purification unless otherwise stated. Deionized water was used wherever necessary.

Table 1. Details of Polymer Characteristics Used in the Present Study

molecular weight, M_n [g/mol]	polydispersity index, M_w/M_n	mole fraction of PS [%]	volume fraction of PDMS, ϕ_{PDMS}	description
10 000	1.05			hydroxyl-terminated PS
9 500	1.10			hydroxyl-terminated PMMA
12 400	1.25	0.58		hydroxyl-terminated PS-*r*-PMMA
5 000	1.07			hydroxyl-terminated PDMS
45 500	1.15	0.60	0.34	cylindrical PS-*b*-PDMS

Polymer Brush Attachment. Substrates (planar and channel cut) were cleaned in a piranha solution (1:3 v/v 30% H_2O_2:H_2SO_4) at 363 K for 60 min, rinsed with deionized water (resistivity ≥18 MΩ cm^{-1}) several times, and dried under N_2. The piranha activation removes any organic contaminant and creates a high density of hydroxyl groups on the silicon substrates. Polymer brush solutions (1.0 wt % in toluene) were used and mixed brush solutions (50:50 volume mixtures) were prepared by addition. The brush solutions were spin-coated onto the substrates at 3000 rpm for 30 s. Samples were annealed in a vacuum oven (Townson and Mercer EV018) at 443 K under vacuum for 6 h. This procedure provides chemically anchored brushes by condensation reactions between −OH groups at the substrate surface and on the brush. Unbound polymers were removed by sonication (Cole-Palmer Model 8891 sonicator) and rinsing in toluene.

Preparation of BCP Thin Films. Thin films of PS-*b*-PDMS were prepared by spin coating (3200 rpm and 30 s) a 1.0 wt % toluene solution of the BCP onto the brush layer. As-cast films were solvent-annealed in glass jars under a saturated toluene environment at room temperature (∼288 K) for 30 min or 3 h. Samples were removed from the glass jars after the desired anneal time and allowed to evaporate the trapped solvent under ambient conditions.

Etch Processes and Pattern Transfer to Silicon. Following BCP film formation, atomic force microscopy (AFM) cannot readily show the microphase-separated structure, because of the presence of a surface wetting layer of PDMS, which must be removed to reveal the BCP arrangement.[21,22] Thus, an etch process (ETCH1) was developed to reveal the PS-*b*-PDMS pattern. This etch was one component of a multistep process that allowed pattern transfer to the substrate. Solvent-annealed PS-*b*-PDMS films were first treated with a CF_4 (15 sccm) plasma for 5 s to remove any surface PDMS layer. This was followed by an O_2 (30 sccm) plasma for 10 s with an inductively coupled plasma (ICP) and reactive ion etching (RIE) powers of 1200 and 30 W, respectively, at 2.0 Pa with a helium backside cooling pressure of 666.6 Pa. These steps follow a similar methodology developed by Ross et al.[22] The process removes the PS component and forms an oxidized form of PDMS on the substrate. The oxidized PDMS cylinders were then used as an etch mask for pattern transfer (i.e., ETCH2). This second processing methodology involves a CHF_3 (80 sccm) and Ar (30 sccm) plasma etch for 5 s with an ICP and RIE powers of 400 and 30 W, respectively, at 1.6 Pa to remove any residual PDMS wetting layer at the substrate surface. This milder etch treatment is critical and needed careful optimization. It is used to remove passive silica and any PDMS components at the silicon substrate surface without removing the "etch mask" formed by the oxidized PDMS cylinders. This process was followed by a selective silicon etch using CHF_3 (80 sccm) and SF_6 (15 sccm) gases for 15 s with an ICP and RIE powers of 1200 and 30 W, respectively, at 2.0 Pa with a helium backside cooling pressure of 1333.2 Pa to transfer the patterns into the underlying substrate. The etching processes were accomplished in an OIPT Plasmalab System100 ICP180 etch tool.

The detailed self-assembly steps starting with PDMS−OH brush grafting, resultant structure formation, and sequential etching steps are schematically shown in Scheme 1. Microphase separation of PS-*b*-PDMS results in a morphology where the PDMS cylinders in a PS matrix are buried underneath a wetting PDMS layer.[21,22]

Characterization of Brush and BCP Films. Advancing contact angles (θ_a) of deionized water on the substrates were measured using a Data Physics Contact Angle (Model OCA15)

Scheme 1. Schematic of the Process Flow Depicting PS-*b*-PDMS Self-Assembly on Silicon Substrate Precoated with PDMS−OH Homopolymer Brush and Subsequent Plasma Etching to Remove the PDMS Wetting Layer, PS Matrix, and Pattern Transfer to the Underlying Silicon[a]

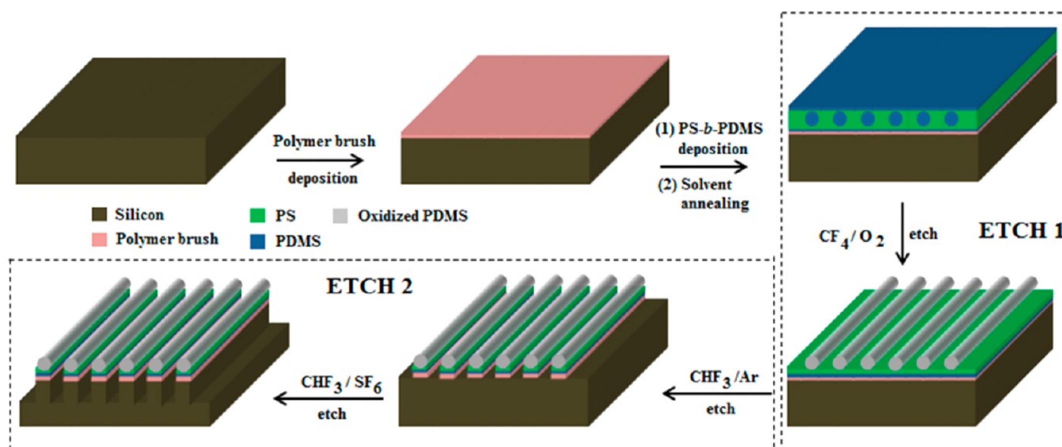

[a]See text for details.

goniometer. Contact angles were measured on the opposite edges of at least three drops and averaged. The values were reproducible to within 1.5°. BCP thin film thicknesses were determined by ellipsometry (Plasmos Model SD2000 Ellipsometer). An average of three readings collected from different locations on a sample surface was used as the film thickness result. A Varian Model IR 610 infrared spectrometer was used to record the FTIR spectra in transmission mode. The measurements were performed in the spectral range of 4000−500 cm^{-1}, with a resolution of 4 cm^{-1}, and data were averaged over 32 scans. Top-down and cross-sectional scanning electron microscope (SEM) images of etched samples were obtained by a high-resolution (<1 nm) field-emission Zeiss Ultra Plus-Scanning Electron Microscope with a Gemini column operating at an accelerating voltage of 5 kV. An FEI Strata 235-Focused Ion Beam (FIB) tool was used to generate FIB lamellae cross sections. E-beam-produced platinum was deposited at the substrate, followed by the ion-beam-deposited platinum. Milling and polishing of the samples were carried out at the lower aperture size and the specimen was imaged under the higher-resolution Zeiss Ultra Plus-SEM.

■ RESULTS

Self-assembly of PS-*b*-PDMS on PDMS−OH Brush. The PDMS−OH brush (thickness of ~4.3 nm, as measured by ellipsometry) ensures that the self-assembly in the PS-*b*-PDMS film results in wetting PDMS layers at the surface and substrate interface.[22] The formation of this sandwich structure will strongly promote the formation of a microphase-separated pattern, where the cylinders are orientated parallel to the surface plane since any vertical orientation will lead to increases in surface energy. Figure 1a shows oxidized PDMS cylinders (as revealed by ETCH1) obtained from the microphase-separated PS-*b*-PDMS films deposited on the PDMS−OH brush. The cross-section SEM image presented in Figure 1b for a single monolayer of PDMS cylinders clearly demonstrates the efficacy of the etch chemistry to reveal the cylindrical patterns.

It is evident from the data in Figure 1 that well-ordered phase separation is seen over macroscopic distances. The mean PDMS cylinder spacing, L_0, and line width, $\langle d \rangle$, were found to be 33.4 and 16.2 nm, respectively. It can be seen from the cross-section image that the oxidized PDMS domains have become rounded during the ETCH1 process, indicating that it is partially isotropic. The oxidation of the PDMS cylinders during this pre-etch step is confirmed by FTIR with the detection of a Si−O−Si signal at 1098 cm^{-1},[24] as displayed in Figure 1c. Dewetting is a major issue with PS-*b*-PDMS system, leading to multilayer pattern formation in some locations on the substrate. Indeed, even with the use of the PDMS−OH brush, a poor coverage of ~60% of the overall substrate area is observed (Figure 1d). The oval/round-shaped areas (islands) in Figure 1d are dewetted regions of BCPs that have a domelike structure, as shown by AFM topography (not shown for the sake of convenience). This dewetting is not due to an incoherent brush layer (Figure 1e) as the brush appears to be very homogeneous without any obvious signs of island formation/defect sites. The consequences of dewetting causing multilayer formation can be observed in Figure 1f. Multilayers of PDMS cylinders can be seen in the cross-section SEM image. It is evident that the upper PDMS cylinders are well-ordered from top-down images but the structure and order within lower layers requires cross-sectional images. The high-resolution FIB cross-section SEM image in Figure 1f provides such data. The FIB data clearly shows the multilayer stacking of cylinders and suggest that order is seen in both the in-plane and out-of-plane cylinder arrangements. The image further reveals the presence of the expected wetting PDMS layer is unaffected by the CF_4 and O_2 etches. The wetting layer is significantly thicker (~8 nm), compared to the thickness of the PDMS−OH brush layer (~4 nm), and strongly suggests that a strong PDMS−OH (brush)−PDMS (BCP) interaction exists and is the cause of the relatively thick wetting layer at this interface.

Surface Characteristics of Different Polymer Brushes. As briefly detailed above, exploration of alternative (to PDMS−OH-based brushes) brush chemistry has been scantly reported, although Ross et al. studied the effect of a PS−OH brush on PS-*b*-PDMS self-assembly on planar and topographically patterned substrates.[22] A key advantage of these alternative brushes is the reduction in the thickness of the PDMS layer that could form at the substrate interface. Here, this work is extended toward PS−OH, PMMA−OH, HO-PS-*r*-PMMA brushes, and combinations thereof. First, the influence of the

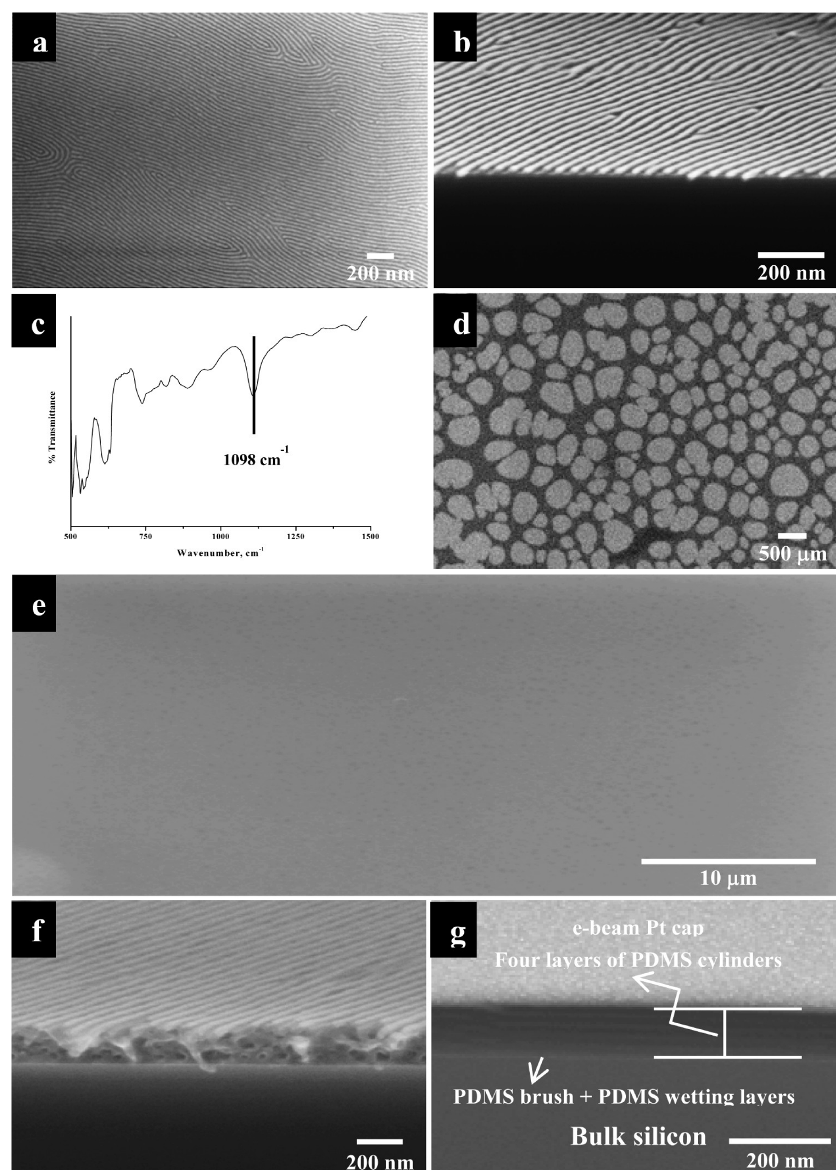

Figure 1. (a) Top-down SEM images of the PS-*b*-PDMS pattern (as revealed by ETCH1), formed using a 3 h solvent anneal on PDMS−OH-brush-modified silicon substrates. (b) Cross-sectional SEM image showing monolayer of PDMS cylinders. (c) FTIR spectrum of the oxidized PDMS cylinders formed from the PS-b-PDMS using ETCH1. (d) SEM image of microphase-separated PS-*b*-PDMS film showing the poor wetting and low film coverage. (e) SEM image of PDMS−OH-brush-anchored silicon substrate. (f) Cross-sectional SEM image and (g) focused-ion-beam (FIB) cross-sectional SEM image of etched PS-*b*-PDMS films, showing multiple layers of PDMS cylinders.

brush type on the water contact angle of the brush layer on planar silicon substrates is summarized in Table 2. The static water contact angle of as-received silicon substrate is found to be ∼45°, which is reduced significantly to 30° on piranha treatment. This is consistent with the piranha activation creating silanol−OH groups, making the surface more hydrophilic with a lower contact angle. All the brushes increase the contact angle of the surface from that of the piranha-treated surfaces by significant amounts. As might be expected, from known solvent parameters, etc.,[25] the PDMS−OH brush has the highest contact angle (most hydrophobic) and the PMMA−OH brush the lowest and the others between those values. The HO-PS-*r*-PMMA brush has an average value of the individual PS−OH and PMMA−OH brushes while the HO-PS-*r*-PMMA and PMMA−OH brush mixture has a value between the values of the individual components. However, the mixed brush systems containing the PS−OH brush all give contact angles of ∼100°, which are near that of the PS−OH alone. This might be explained because the PS−OH brush film thickness is significantly greater than that of the other brushes (Table 2) and suggests that the chemistry of the surface is dominated by the thicker PS component.

FTIR measurements can provide evidence about the presence of the polymer brushes and qualitative information about relative concentrations, based on the intensity of the peaks. Typical FTIR data of the polymer brushes on silicon substrates are shown in Figure 2, and bands that can be associated with both the polymer films and the substrate (marked in the figure) can be observed. The FTIR spectrum of the PDMS−OH-brush-anchored silicon substrate (Figure 2a) show a well-resolved Si−O−Si vibration band near 1098 cm^{-1}, indicative of silica materials.[24] The high intensity of the vibration band is due to high silicon content of the polymer brush, which is ∼36%, based on its molecular weight. However,

Table 2. Water Contact Angle and Film Thickness Data of Polymer Brush and Diblock Copolymer Films on Silicon Substrates

surface finish	contact angle (± 1.5°)	film thickness	film thickness brush and BCP
SiO_2/Si (as received)	44.7°		
SiO_2/Si (piranha)	29.5°		27.3 nm
PS–OH	97.9°	7.3 nm	33.6 nm
PMMA–OH	78.6°	4.5 nm	30.8 nm
HO-PS-*r*-PMMA	83.2°	5.8 nm	32.4 nm
PDMS–OH	112.6°	4.3 nm	31.6 nm
PS–OH + PMMA–OH	100.8°	6.5 nm	32.8 nm
PS–OH + HO-PS-*r*-PMMA	99.2°	6.3 nm	33.1 nm
PMMA–OH + HO-PS-*r*-PMMA	79.2°	4.3 nm	30.5 nm
PS–OH + PMMA–OH + HO-PS-*r*-PMMA	100.0°	5.9 nm	32.6 nm

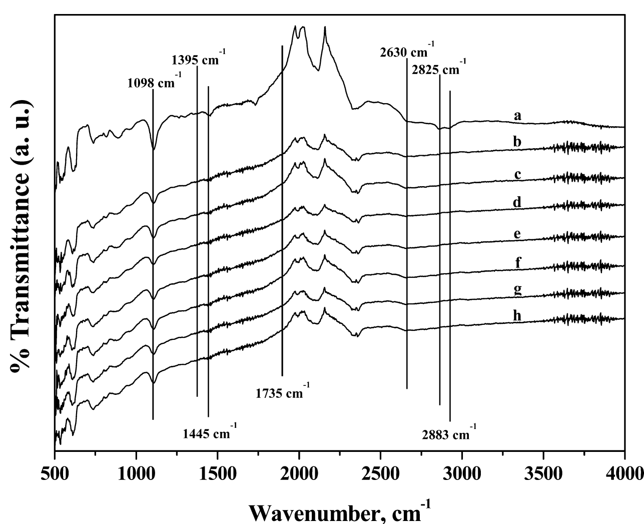

Figure 2. FTIR spectra of (a) PDMS–OH, (b) HO-PS-*r*-PMMA, (c) PS–OH, (d) PMMA–OH, (e) PS–OH + PMMA–OH, (f) HO-PS-*r*-PMMA + PS–OH, (g) HO-PS-*r*-PMMA + PMMA–OH, and (h) HO-PS-*r*-PMMA + PS–OH + PMMA–OH polymer-brush-anchored planar silicon substrates after cleaning.

there may be a minor contribution from the native oxide layer of the silicon substrate, as seen below. The FTIR spectrum of the brush layer also shows a medium-strength OH valence vibration band near 2630 cm^{-1}. The presence of the OH band is probably due to hydroxylation and attached water through hydrogen bonding. The peaks observed at 1395, 2825, and 2883 cm^{-1} can be assigned to CH_3, CH_2, and CH stretching vibrations,[25] respectively.

FTIR spectra of other polymer brushes are presented in Figure 2 and also reveal the presence of a Si–O–Si vibration band near 1098 cm^{-1}, indicative of silica materials. Since these polymers are non-silicon-containing, it is clear that these features arise from the underlying SiO_2 at the silicon substrate. Note, however, that intensity of this band is much weaker than in the data of the PDMS–OH brush and suggests that the contribution of silicon oxide type species following ETCH1 are much more significant, compared to that of SiO_2 from the substrate. Other vibrational bands from the polymer brushes are difficult to observe, but bands associated with CH_3, CH_2, and CH stretching vibrations can be identified at 1395, 2825, and 2883 cm^{-1}. The rather low intensity of these features is consistent with the presence of the thin brush layers (see Table 2). A C–CH_3 deformation band was observed at 1445 cm^{-1} in all the spectra. The C═O stretching vibration band arising from the PMMA–OH and HO-PS-*r*-PMMA and their combinations with/without PS–OH brush could be detected at 1735 cm^{-1}.[26] However, the C–O–C stretch usually observed at 1105 cm^{-1}[26] could have merged with the Si–O–Si band. Though the presence of the polymer brushes was evidenced from the FTIR, it could not reveal the relative concentrations of the brushes and any preferential grafting in the brush combinations. XPS might provide greater quantifiable analysis of these mixed brush-modified surfaces. However, in our experiments, it added little, because of the much larger C 1s signals from aryl and aliphatic carbon signals.

The brush-treated surfaces were further characterized using ellipsometry, and the results are presented in Table 2. The thickness of the brush layers lies in the range of 4–7 nm and is in the range expected from simple calculations. Polystyrene (PS) and polymethylmethacrylate (PMMA) adopt a random coil structure and is modeled by $\langle h^2\rangle_0 = M_w \times 0.43$ and $\langle h^2\rangle_0 =$

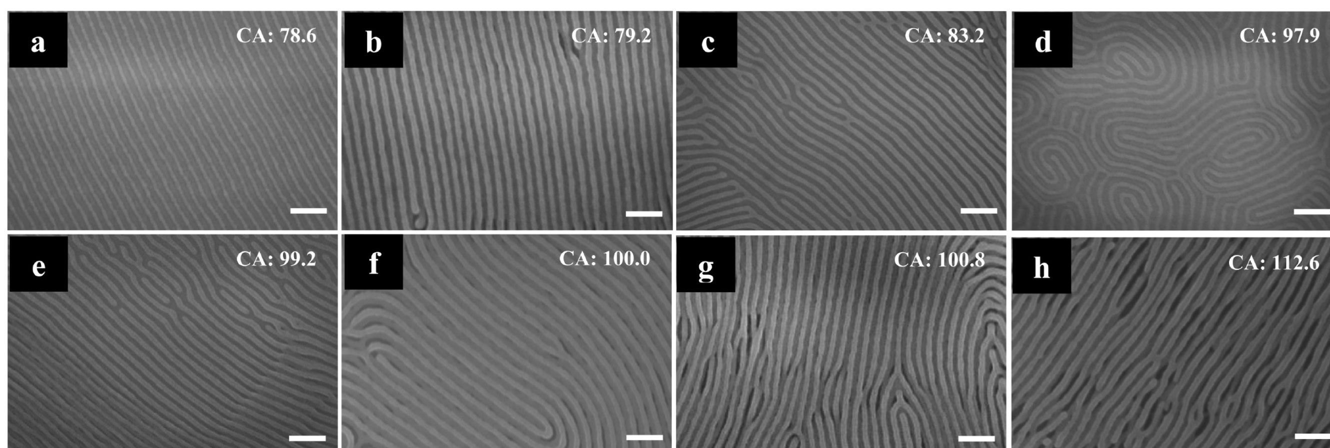

Figure 3. Top-down SEM images (image scale bar = 100 nm) of microphase-separated PS-*b*-PDMS films, as revealed by ETCH1 on the following modified substrates: (a) PMMA–OH, (b) HO-PS-*r*-PMMA + PMMA–OH, (c) HO-PS-*r*-PMMA, (d) PS–OH, (e) HO-PS-*r*-PMMA + PS–OH, (f) HO-PS-*r*-PMMA + PS–OH + PMMA–OH, (g) PS–OH + PMMA–OH, and (h) PDMS–OH brush-coated silicon substrates. Data were recorded after a 30 min solvent anneal.

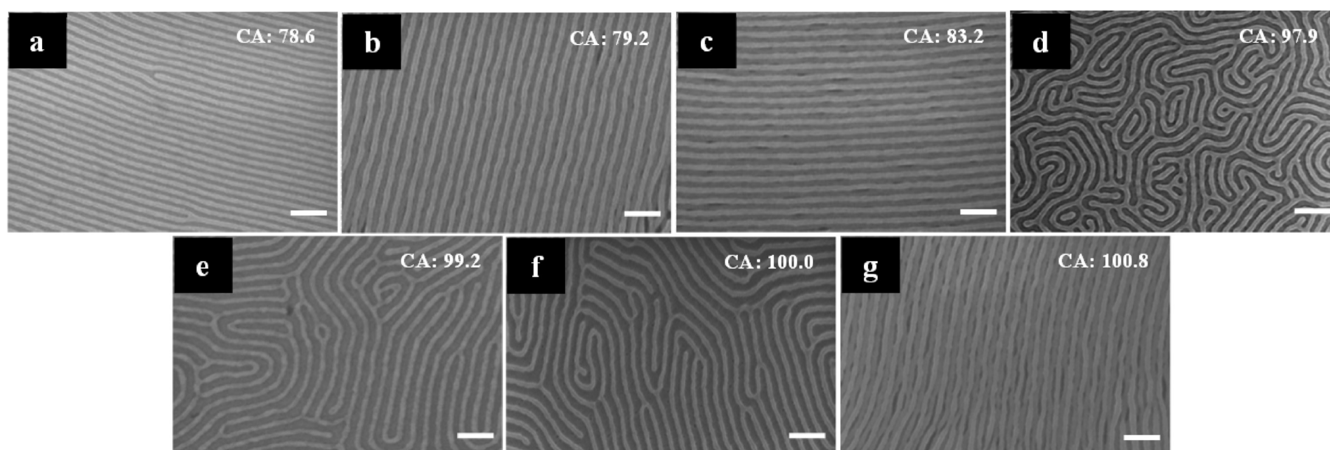

Figure 4. Top-down SEM images (image scale bar = 100 nm) of microphase-separated PS-*b*-PDMS films, as revealed by ETCH1 on (a) PMMA−OH, (b) HO-PS-*r*-PMMA + PMMA−OH, (c) HO-PS-*r*-PMMA, (d) PS−OH, (e) HO-PS-*r*-PMMA + PS−OH, (f) HO-PS-*r*-PMMA + PS−OH + PMMA−OH, and (g) PS−OH + PMMA−OH brush-coated silicon substrates. Data were recorded after a 3 h solvent anneal.

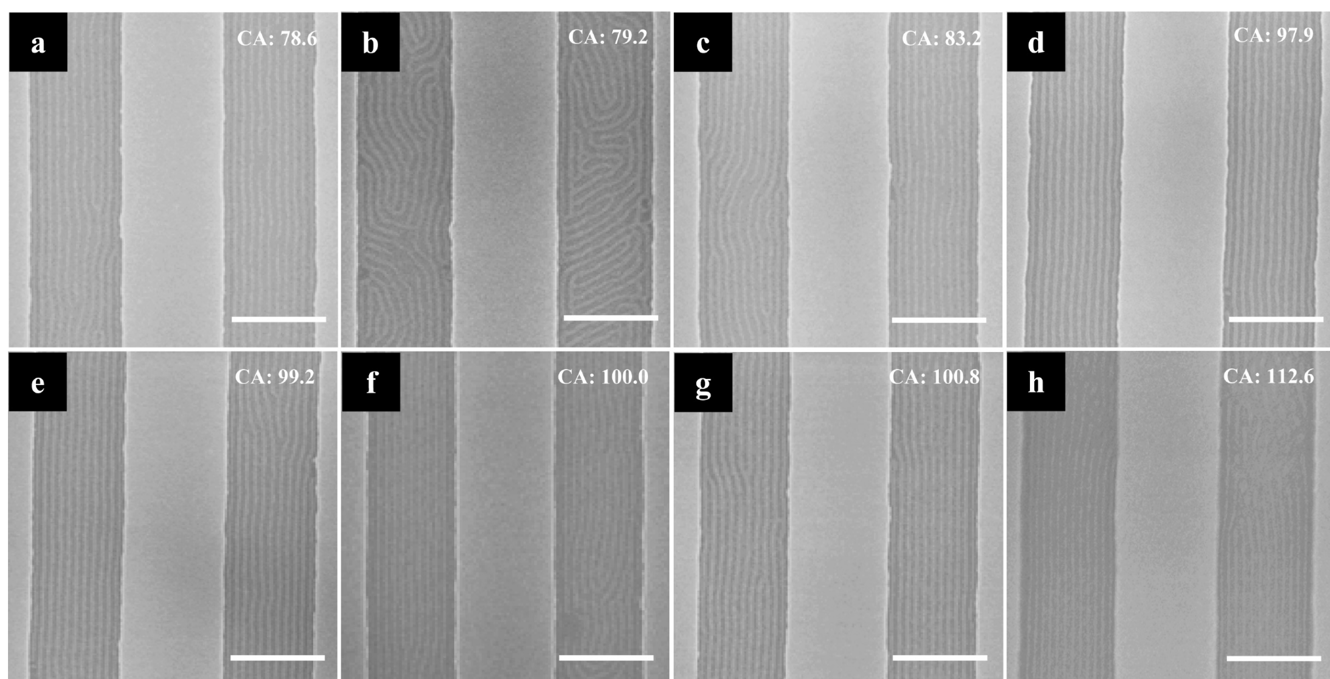

Figure 5. Top-down SEM images (image scale bar = 300 nm) of microphase-separated PS-*b*-PDMS films, as revealed by ETCH1 on (a) PMMA−OH, (b) HO-PS-*r*-PMMA + PMMA−OH, (c) HO-PS-*r*-PMMA, (d) PS−OH, (e) HO-PS-*r*-PMMA + PS−OH, (f) HO-PS-*r*-PMMA + PS−OH + PMMA−OH, (g) PS−OH + PMMA−OH, and (h) PDMS−OH brush-coated patterned substrates. The solvent anneal time was 30 min.

$M_w \times 0.42$, respectively, where $\langle h^2 \rangle_0$ is the mean-square end-to-end distance of the polymer coil and M_w is the molecular weight.[27] The random coil size estimated for PS−OH and PMMA−OH are 6.6 and 6.3 nm, respectively, compared to measured sizes of 7.3 and 4.5 nm, respectively. The coil size calculated for HO-PS-*r*-PMMA considering $\langle h^2 \rangle_0 = M_w \times 0.425$ and found to be 7.3 nm (experimental value = 5.8 nm). Assuming $\langle h^2 \rangle_0 = M_w \times 0.425$ for PDMS−OH, the value estimated is 4.6 nm and measured value is 4.3 nm. These data are in reasonable agreement with the measured brush layer thickness, since some surface strain/relaxation in the thin film is expected. This would suggest that a complete monolayer of polymer molecules is formed from the brush procedure used here and provides an excellent surface for BCP deposition. The PS−OH brush shows significantly greater thickness than that estimated by ellipsometry, suggesting distortions in the random coil structure. The thickness values for the mixed brushes seem to have values between those of the two components and are consistent with attachment of both polymers rather than preferential adsorption and reaction of one component.

Effect of Polymer Brushes on PS-*b*-PDMS Self-Assembly. Microscopic examination of BCP films on the brush-modified surfaces suggest that exposure to the solvent anneal process for longer periods can lead to significant dewetting,[28] and coverages on, e.g., the PDMS−OH brush drop from ∼90% (30 min) to ∼60% (3 h). In this way, any structures are best viewed as metastable. Thus, in this work, shorter (30 min) and longer (3 h) anneal times were investigated to understand their effect on microphase separation. Generally, the non-PDMS-based brushes showed

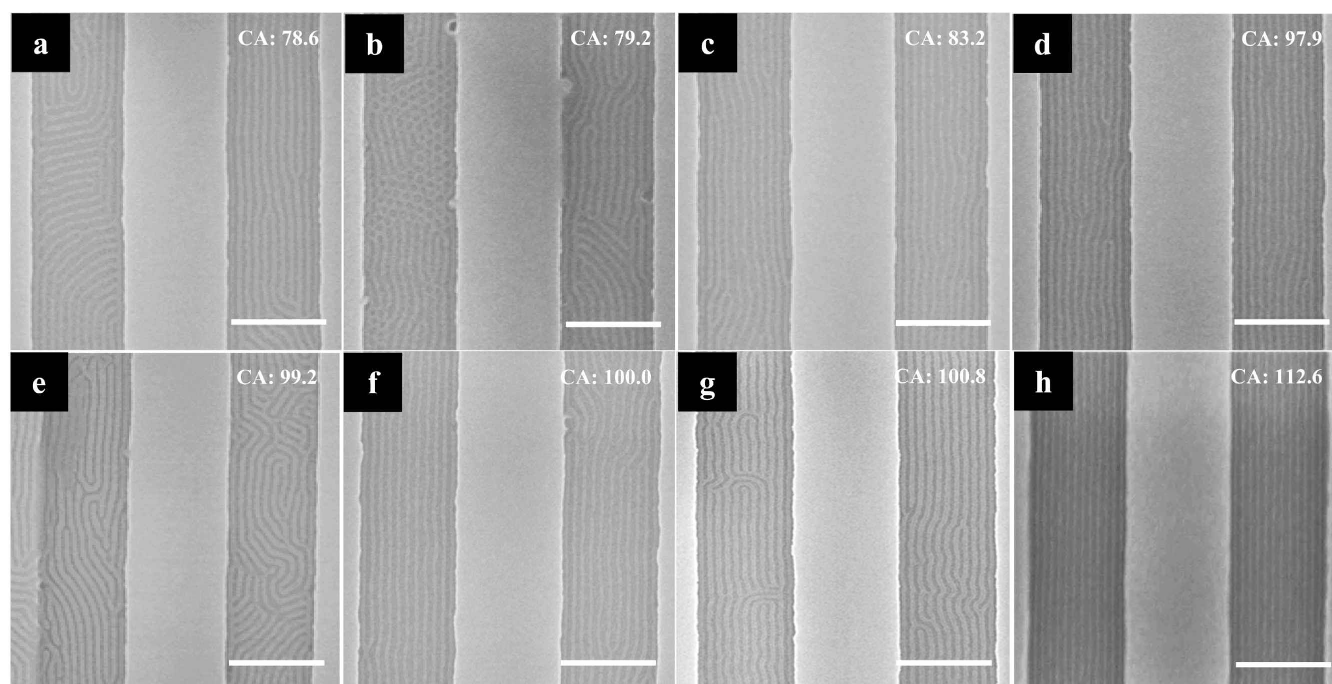

Figure 6. Top-down SEM images (image scale bar = 300 nm) of microphase-separated PS-*b*-PDMS films, as revealed by ETCH1 on (a) PMMA−OH, (b) HO-PS-*r*-PMMA + PMMA−OH, (c) HO-PS-*r*-PMMA, (d) PS−OH, (e) HO-PS-*r*-PMMA + PS−OH, (f) HO-PS-*r*-PMMA + PS−OH + PMMA−OH, (g) PS−OH + PMMA−OH, and (h) PDMS−OH brush-coated patterned substrates. The solvent anneal period was 3 h.

coverages of >80%−90%, even after the longer anneal time, and this is a key advantage of their use. The effect of anneal time was combined with the effect of surface treatment by different polymer brushes, and the results are presented in Figures 3 and 4, for 30 min and 3 h, respectively.

SEM images were taken at different locations on the substrate and show that the orientation is homogeneous over the entire surface. Representative images are shown in the figures. On first examination, the data from the 30 min and 3 h solvent anneal times are essentially similar with well-ordered films formed of parallel cylinder orientation. However, if these are examined closely, it can be seen that some images consist of multilayer features as described above. This can be seen in Figures 3f−h, where dark areas can be seen due to stacked cylinders exposed by the etch treatment. As discussed earlier, these multilayer regions exist because of dewetting and formation of island structures. It is apparent that this dewetting behavior is more likely at the surfaces of higher contact angle (i.e., more hydrophobic). For longer solvent-anneal periods, dewetting is generally increased and in several cases multilayer formation is visible at lower contact angles (78.6°, 79.2°, and 83.3°). However, surfaces displaying contact angles of 97.9° and 99.2° were resistant to dewetting (PS−OH and PS−OH + HO-PS-*r*-PMMA brushes). It is suggested that these surfaces have optimal properties for interaction with the PS-*b*-PDMS BCP.

Directed Self-Assembly by Graphoepitaxy. As discussed earlier, surface treatment with polymer brushes facilitates self-assembly, short-range domain ordering, defect minimization, and improves the wetting property of the BCP. However, to achieve long-range pattern ordering, this surface treatment can be combined with the graphoepitaxy technique to direct self-assembly in PS-*b*-PDMS and has been demonstrated in several articles.[22,29,30] These topographically patterned surfaces are also extremely useful in understanding the changes in surface chemistry that has been varied by use of the various polymer brushes. This is because top-down imaging can be used to determine preferred block orientation at the sidewall. As above, the patterned substrates were precoated with different hydroxyl-terminated polymer brushes and their mixtures in different combinations prior to BCP deposition. Figures 5 and 6 show the results of the PS-*b*-PDMS pattern after ETCH1, following a short and long solvent anneal. It can be seen from Figures 5 and 6 that the brushes are all generally compatible with graphoepitaxial alignment of the PS-*b*-PDMS. Generally, for the hexagonal structure, preferred alignment should be achieved when the sidewalls preferentially interact with the majority block, compared to the minor component. If the sidewalls are neutral and interact equally with both blocks (thus favoring the presence of both blocks at the sidewall), a nonaligned structure is formed. For the samples solvent annealed for 30 min, it is only the mixture of PMMA−OH and HO-PS-*r*-PMMA brushes that leads to poor alignment and functionality at the wall that could be described as neutral. For the 3 h solvent anneal, the quality of the alignment seems to be significantly worse for most samples and more defects can be seen in the images presented in Figure 6. However, this is not easy to quantify, because a majority of the defects observed arise from defects in the sidewall, which cause local variations in the channel width. However, neutral-type alignment can be clearly seen in the data recorded for the PMMA−OH and the combined PMMA−OH and HO-PS-*r*-PMMA brush layers. It should also be noted that the data from the combined HO-PS-*r*-PMMA brush system also shows mixed morphology with regions of vertical and perpendicular alignment of the cylinders. This does confirm neutrality of the sidewall and suggests the PMMA−OH/HO-PS-*r*-PMMA base is neutral enough to allow some vertical alignment of the cylinders.

Pattern Transfer of PS-*b*-PDMS Films into the Underlying Substrate. To demonstrate the usefulness of this system

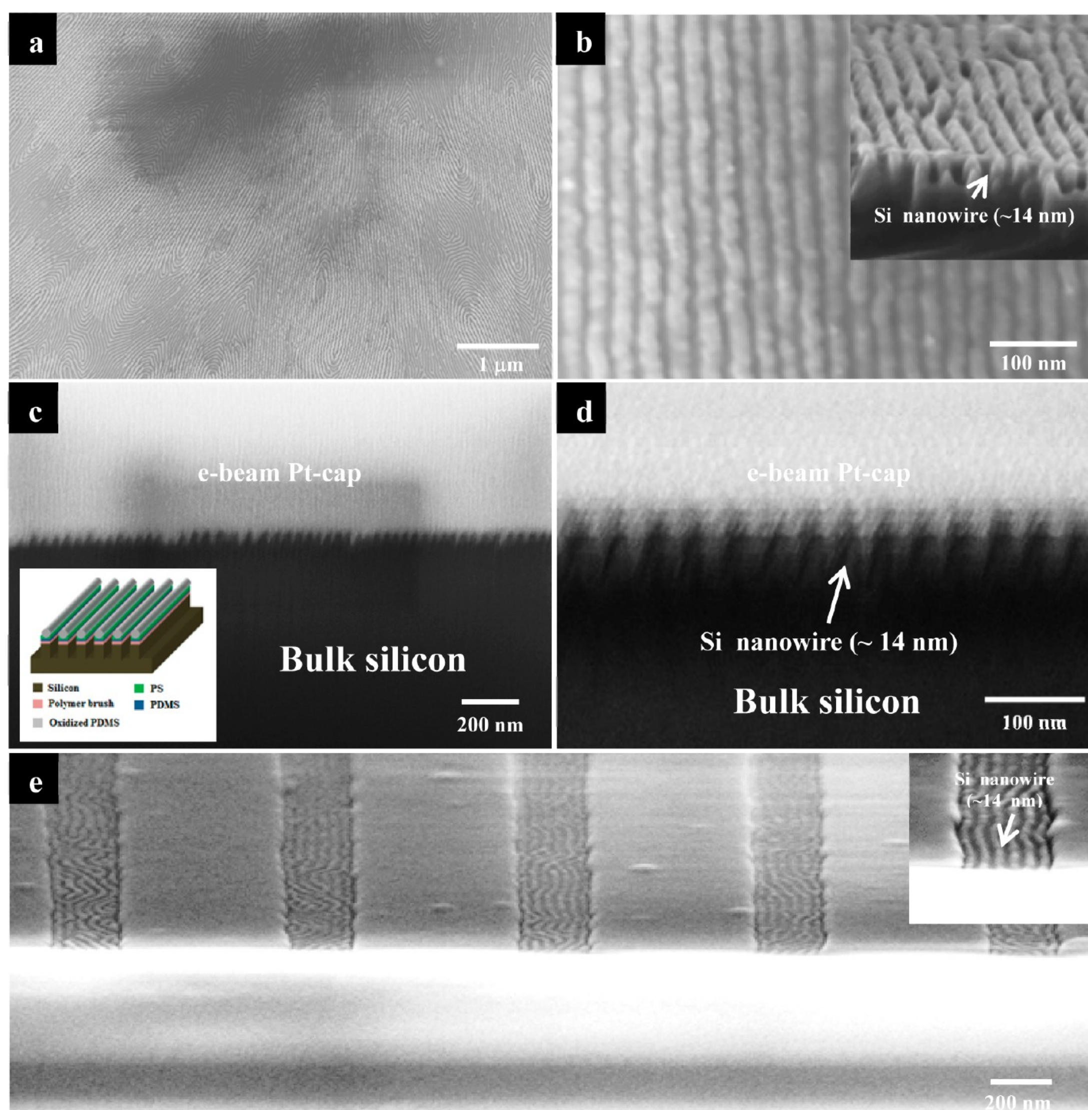

Figure 7. (a) Low-resolution and (b) high-resolution top-down SEM images of PDMS cylindrical patterns transferred to underlying silicon substrate. The inset of panel b is a corresponding cross-section SEM image. (c) Low-resolution and (d) high-resolution FIB cross-sectional SEM images of PDMS cylindrical patterns transferred to the underlying silicon substrate. The inset of panel c is a schematic showing oxidized PDMS cylinders on silicon nanowires. (e) Tilted SEM image of PDMS cylindrical patterns transferred to the underlying SiO_2 on a topographically patterned substrate (the inset to panel e is a corresponding high-resolution SEM image).

for application in microelectronic fabrication, the patterns obtained following ETCH1 were pattern transferred into the substrate (ETCH2). The pattern transfer of PS-*b*-PDMS BCP to the substrate is not a straightforward process, unlike that for more well-established polymer systems, e.g., PS-*b*-PMMA,[23,31] and PS-*b*-PEO,[32] because of the complex structure of the PS-*b*-PDMS films. It should be noted that, for an effective pattern transfer process, the O_2 etch used in ETCH1 must be carefully optimized, so that the cylinder structure is not undercut. However, if this is achieved, the oxidized, silica-like cylinders can act as a hard mask for pattern transfer. Figure 7a and 7b shows the top-down and cross-sectional SEM images of the silicon nanowires on the silicon substrate obtained after the etches were used to remove the silica-like materials at the substrate surface and then to selectively remove silicon. The cross-sectional SEM image shows the nanowire line width of ~14 nm with a pattern depth of ~26 nm. The FIB cross-sectional SEM images shown in Figures 7c and 7d provide a more-detailed image of the silicon nanowires fabricated in this way. The silicon features on the substrate are slightly narrower than the width of the initial oxidized PDMS cylinders, because of a partly isotropic etching process. A reasonable aspect ratio of ~1.3 was obtained. The tilted and cross-sectional SEM images of the silicon nanowires on the topographically patterned silicon substrate are shown in Figure 7e. The silicon nanowires formed are aligned within the channel and appear to be reasonably smooth. The tilted SEM images (Figure 7e and inset image) show that the pattern transfer process is successful with a line width of ~13.6 nm and a pattern depth of ~25.3 nm, consistent with that recorded from the planar substrate.

■ DISCUSSION AND CONCLUSIONS

The first conclusion of this work is that the choice of a suitable interfacial brush for control of BCP orientation is not facile and choices may require very careful consideration if wetting layers are to be avoided or if the brush is to be used within topographically patterned substrates for alignment control. It might be imagined that a PDMS−OH brush would be an ideal

choice for this system; however, in terms of wetting characteristics, it is far from ideal and, indeed, island-like structures are observed as solvent anneal times increase. The reason for this might lie in the surface roughness of the surfaces with this island structure. Because of the greater surface area, the surface energy will be significantly reduced because of the increased area of the low-surface-energy PDMS wetting layer that forms in these systems. As the surfaces are made less hydrophobic, wetting appears to improve, which seems to be counterintuitive. However, this may be because they favor the PS component and prevent a PDMS interface layer from forming. Multilayer formation seems, once again, to become more likely at the lowest contact angles, suggesting the BCP brush layer are becoming less favorable again. It is clear that rationalizing these effects on just water contact angle is not possible. Instead, the chemical interaction of a brush and the BCP as well as the structure of the film must be considered. Here, it might be suggested that regular thickness, coherent films are more likely to be formed when the brush has a majority PS component and this must be because of favorable PS−PS interactions at the brush−BCP interface. At the most hydrophilic surfaces, i.e., those based on majority PMMA−OH systems, the system favors neither PS nor PDMS and island formation becomes probable. However, despite the complexity, the correct choice of brush can allow highly coherent films of regular thickness to be formed. Importantly, the formation of a PDMS wetting layer can be avoided with the correct choice of brush.

While the brush can be chosen to control wetting phenomena on planar surfaces, it also influences the regularity of DSA structures formed in topographically patterned substrate surfaces. However, an important point to note is that optimal surface wetting may not be consistent with the greatest structural alignment. In this system, it appears that wetting is favored by having a surface that is less favorable to PDMS, but it appears from the data that the most hydrophobic surfaces lead to surface neutrality and alignment is decreased and the number of pattern defects increases.

Tuning the surface chemistry in this system is important for the possible applications described herein whereby ultrasmall features can be created for device development. The presence of multilayers due to wetting cannot be tolerated because pattern transfer results in complex 3-D structures. Furthermore, a surface PDMS wetting layer is not favored (but note, even with this layer pattern transfer may be achieved), because it introduces additional (silica removal) steps, which compromises the function of the polymer-derived structure as an on-chip etch mask, and achieving high selectivity and good aspect ratio of the formed silicon features is difficult.

Thus, it seems that very fine control of surface chemistry is required to optimize several factors that are not necessarily compatible. The number of well-optimized surface chemistries for the DSA of BCP systems is relatively few. This work demonstrates that simple contact angle comparisons are not sufficient to predict behavior and considerable further work is needed to provide a definitive understanding of surface functionalization to control pattern formation as well as to provide methods by which the correct surface chemistry might be predicted from standard analytical methods.

AUTHOR INFORMATION

Corresponding Author

*Tel.: +353 214902180. Fax: +353 214274097. Email: m.morris@ucc.ie.

Notes

The authors declare no competing financial interest.

ACKNOWLEDGMENTS

Financial support for this work is provided by the EU FP7 NMP project, LAMAND (Grant No. 245565) project, and the Science Foundation Ireland, CRANN CSET grant, and is gratefully acknowledged.

REFERENCES

(1) Wissen, M.; Bogdanski, N.; Moellenbeck, S.; Scheer, H.-C. In *Strategies for Hybrid Techniques of UV Lithography and Thermal Nanoimprint*; IEEE: New York, 2008.

(2) Chung, S.; Felts, J. R.; Wang, D.; King, W. P.; De Yoreo, J. J. *Appl. Phys. Lett.* **2011**, *99*, 193101−3.

(3) Grigorescu, A. E.; Hagen, C. W. *Nanotechnology* **2009**, *20*, 292001−31.

(4) Namatsu, H.; Watanabe, Y.; Yamazaki, K.; Yamaguchi, T.; Nagase, M.; Ono, Y.; Fujiwara, A.; Horiguchi, S. *J. Vac. Sci. Technol. B* **2003**, *21*, 1−5.

(5) Hirai, Y.; Hafizovic, S.; Matsuzuka, N.; Korvink, J. G.; Tabata, O. *J. Microelectromech. Syst.* **2006**, *15*, 159−168.

(6) Hamley, I. W. *Angew. Chem., Int. Ed.* **2003**, *42*, 1692−1712.

(7) Mack, C. A. *IEEE Trans. Semiconduct. Manufact.* **2011**, *24*, 202−207.

(8) Freebody, M. *Photon Spectra* **2011**, *45*, 45−47.

(9) Kumar, P. *Nanoscale Res. Lett.* **2010**, *5*, 1367−1376.

(10) Ariga, K.; Hill, J. P.; Lee, M. V.; Vinu, A.; Charvet, R.; Acharya, S. *Sci. Technol. Adv. Mater.* **2008**, *9*, 014109.

(11) Hawker, C. J.; Russell, T. P. *MRS Bull.* **2005**, *30*, 952−966.

(12) Guo, L. J. *Adv. Mater.* **2007**, *19*, 495−513.

(13) Gates, B. D.; Xu, Q.; Stewart, M.; Ryan, D.; Willson, C. G.; Whitesides, G. M. *Chem. Rev.* **2005**, *105*, 1171−1196.

(14) Mårtensson, T.; Carlberg, P.; Borgström, M.; Montelius, L.; Seifert, W.; Samuelson, L. *Nano Lett.* **2004**, *4*, 699−702.

(15) Chou, S. Y.; Krauss, P. R.; Renstrom, P. J. *Appl. Phys. Lett.* **1995**, *67*, 3114−3116.

(16) Li, H.-W.; Huck, W. T. S. *Nano Lett.* **2004**, *4*, 1633−1636.

(17) Farrell, R. A.; Kehagias, N.; Shaw, M. T.; Reboud, V.; Zelsmann, M.; Holmes, J. D.; Sotomayor Torres, C. M.; Morris, M. A. *ACS Nano* **2011**, *5*, 1073−1085.

(18) Salaün, M.; Kehagias, N.; Salhi, B.; Baron, T.; Boussey, J.; Sotomayor Torres, C. M.; Zelsmann, M. *J. Vac. Sci. Technol. B* **2011**, *29*, 06F208−06F212.

(19) Politakos, N.; Ntoukas, E.; Avgeropoulos, A.; Krikorian, V.; Pate, B. D.; Thomas, E. L.; Hill, R. M. *J. Polym. Sci., Part B: Polym. Phys.* **2009**, *47*, 2419−2427.

(20) Park, S. M.; Liang, X.; Harteneck, B. D.; Pick, T. E.; Hiroshiba, N.; Wu, Y.; Helms, B. A.; Olynick, D. L. *ACS Nano* **2011**, *5*, 8523−8531.

(21) Hobbs, R. G.; Farrell, R. A.; Bolger, C. T.; Kelly, R. A.; Morris, M. A.; Petkov, N.; Holmes, J. D. *ACS Appl. Mater. Interfaces* **2012**, *4*, 4637−4642.

(22) Jung, Y. S.; Ross, C. A. *Nano Lett.* **2007**, *7*, 2046−2050.

(23) Borah, D.; Shaw, M. T.; Rasappa, S.; Farrell, R. A.; O'Mahony, C. T.; Faulkner, C. M.; Bosea, M.; Gleeson, P.; Holmes, J. D.; Morris, M. A. *J. Phys. D: Appl. Phys.* **2011**, *44*, 174012−174024.

(24) Kirk, C. T. *Phys. Rev. B* **1998**, *38*, 1255−1273.

(25) Bernaerts, K. V.; Du Prez, F. E. *Polymer* **2005**, *46*, 8469−8482.

(26) Bodas, D. S.; Mahapatra, S. K.; Gangal, S. A. *Sens. Actuators, A* **2005**, *120*, 582−588.

(27) Fetters, L. J.; Lohse, D. J.; Richter, D.; Witten, T. A.; Zirkel, A. *Macromolecules* **1994**, *27*, 4639−4647.

(28) Yang, J.; Wang, Q.; Yao, W.; Chen, F.; Fu, Q. *Appl. Surf. Sci.* **2011**, *257*, 4928−4934.
(29) Jung, Y. S.; Jung, W. C.; Tuller, H. L.; Ross, C. A. *Nano Lett.* **2008**, *8*, 3776−3780.
(30) Jeong, J. W.; Park, W. I.; Do, L.-M.; Park, J.-H.; Kim, T.-H.; Chae, G.; Jung, Y. S. *Adv. Mater.* **2012**, *24*, 3526−3531.
(31) Farrell, R. A.; Petkov, N.; Shaw, M. T.; Djara, V.; Holmes, J. D.; Morris, M. A. *Macromolecules* **2010**, *43*, 8651−8655.
(32) Ghoshal, T.; Maity, T.; Godsell, J. F.; Roy, S.; Morris, M. A. *Adv. Mater.* **2012**, *24*, 2390−2397.